Defect-Mediated Melting in Superheated Noble Gas Crystals

Francesco Delogu*

Dipartimento di Ingegneria Chimica e Materiali, Università di Cagliari, piazza d'Armi, I-09123 Cagliari, Italy

Received: June 13, 2005; In Final Form: August 20, 2005

Molecular dynamics simulations have been used to investigate the mechanisms governing the homogeneous melting of pure noble gases at the limit of superheating. For each chemical species considered, the heterogeneous melting point was estimated by monitoring the thermal behavior of crystalline systems containing a high-angle grain boundary. To determine the limit to superheating, calculations were instead carried out on a perfect crystalline bulk. The temperature was gradually increased to bring the systems within the metastable region above the equilibrium melting point. The static order parameter was employed to monitor the structural disordering during the slow temperature increase and to determine the temperature at which the crystalline lattice collapses to a liquid. Structural disorder was further characterized by studying the appearance of atoms with defective coordination. Their relative number and spatial correlation appeared to play a fundamental role in destabilizing the crystalline lattice bulk and triggering the homogeneous melting. The fraction of atoms with defective coordination and the total length of the stringlike clusters they form in the vicinity of the homogeneous melting point were found to be approximately the same for all of the chemical species considered. These findings have been compared with theoretical predictions.

Introduction

Melting from the solid to liquid phase is a ubiquitous and familiar process representing one of the rare cases in which a phase transition is fully accessible outside of scientific laboratories.[1,2] As a consequence, it has attracted a great deal of interest for centuries.

From the point of view of classical thermodynamics, the occurrence of melting is fully rationalized in terms of the Gibbs free energy curves of solid and liquid phases,[3] the intersection of which identifies the melting point T_m. Conversely, the mechanism of melting is not yet fully understood. The first attempt to give mechanistic basis to the thermodynamic description of melting dates back to the work of Lindemann at the beginning of the 20th century,[4,5] who predicted the existence of a vibrational instability due to the increasing hindrance vibrating atoms as the temperature increases. About thirty years later, Born demonstrated the existence of a phonon instability marked by the vanishing of the shear moduli.[6,7] The resulting homogeneous melting due to the so-called "rigidity catastrophe" cannot, however, be related to the thermodynamic melting, which takes place at temperatures considerably lower than the one predicted by Born[8] and according to a heterogeneous mechanism.[2,9−11] Homogeneous melting can indeed occur only when the molten phase heterogeneous nucleation is suppressed.[2,12−14] Experimental and theoretical research on superheated crystalline lattices has now shown that the Born elastic instability actually identifies the ultimate limit to crystalline stability.[8] It is indeed preceded by a hierarchy of entropy-, enthalpy-, and volume-driven instabilities. All of these homogeneous processes are preceded, in turn, by the homogeneous nucleation of molten phase in the bulk of the crystalline phase.[15] This latter process represents, therefore, the first limit to crystal superheating.

Despite their intrinsic differences, all of the homogeneous processes mentioned above are expected to be deeply correlated. An indication in this sense has recently come from a numerical study showing that the homogeneous nucleation of the molten phase takes place in vibrationally excited regions of a solid with a contemporary satisfaction of the Lindemann and Born criteria for melting.[16] Along this line, further advance can be obtained by reconciling and unifying the different melting criteria as well as by rationalizing them within a more satisfactory conceptual framework such as the one offered by more recent defect-mediated melting theories.[2] These are regarded as promising frameworks to rationalize melting since the late 1970s, when Kosterlitz, Thouless, Halperin, Nelson, and Young successfully developed the so-called KTHNY theory for the melting of two-dimensional systems.[17−19] In recent years, significant progress has been also obtained in the extension of the KTHNY theory to three-dimensional systems.[20−22] In particular, Burakovsky et al. have shown that the density of dislocation loops at melting is approximately the same for a great number of elemental species.[21] The use of the experimental melting point as a parameter to estimate the dislocation density at melting implies that dislocation loops form according to a heterogeneous melting mechanism. However, the model is clearly referred to a homogeneous melting scenario, as underlined by a successive work relating homogeneous melting to the proliferation of dislocation lines in the bulk.[22]

Addressing this latter point, the present work employs molecular dynamics (MD) simulations to gain a deeper insight into the atomistic processes governing the formation of defective structures and the subsequent melting of the superheated crystal. The study is referred to the Ne, Ar, Kr, and Xe noble gases. For all of these chemical systems, the limit of superheating was properly determined together with the details of dynamics concerning the appearance and interaction of atoms with defective coordination. The results obtained are finally compared with the predictions of the model proposed by Burakovsky et al.[21] The numerical procedures are described in detail in the following.

Molecular Dynamics Simulations. MD calculations were performed on systems of atoms arranged on crystalline lattices

* E-mail: delogu@dicm.unica.it.

10.1021/jp0531715 CCC: $30.25
Published on Web 10/05/2005

TABLE 1: LJ Potential Parameters for the Chemical Species Investigated

element	ϵ, 10^{-21} J	σ, Å
Ne	0.49	2.75
Ar	1.65	3.40
Kr	2.36	3.60
Xe	3.05	4.10

corresponding to the fcc cF4 structure.[23] A conventional 12-6 Lennard-Jones (LJ) pair potential

$$V(r) = r^{-12} - 2r^{-6} \tag{1}$$

was used to describe interactions.[24] Reduced units were used to properly compare the systems investigated. Accordingly, distances are expressed in σ units, energy in ϵ units, and pressure in $\sigma^3\epsilon$ units. The temperature is expressed in $k_B\epsilon^{-1}$ units, where k_B is the Boltzmann constant. The energy well depth ϵ and the LJ diameter σ were suitably set equal to the ones pertaining to Ne, Ar, Kr, and Xe chemical species. Their values are reported in Table 1. The elementary cell constant a_0 was defined by the relationship $a_0 = 2^{1/2}r_0$, where $r_0 = 2^{1/6}$. σ is the equilibrium nearest-neighbors distance at 0 K. Forces were computed for distances r extending to a spherical cutoff radius $r_c = 3\sigma$, approximately corresponding to the ninth shell of neighbors.

MD calculations were carried out within the Nosè-Andersen *NPT* ensemble, i.e., at number of atoms N, pressure P, and temperature T constant.[25,26] The Parrinello−Rahman scheme, which permits the study of phase transformations with crystallographic cell shape change, was also implemented.[27] The equations of motion were solved by employing a fifth-order predictor−corrector algorithm and a time step $\delta t = 5$ fs.

Heterogeneous Melting. The thermodynamic melting point T_m was evaluated for each system investigated by applying the methodology discussed in previous works.[28,29] Such a procedure is necessary in light of the fact that the equilibrium melting point T_m, determined by means of numerical simulations, can be significantly different from the one experimentally observed, depending on both the interatomic potential employed and the simulation conditions.[28,29] For these reasons, to estimate the equilibrium melting point T_m, numerical simulations were performed on systems containing a (γ29) high-angle twist boundary obtained by rotating two perfect semicrystals with (001) faces of an angle $\theta = 43.6°$. The simulation cell was chosen to contain 32 (001) lattice planes, with 29 atoms in each plane. The cell consisted, then, of 928 atoms. The grain boundary occupied the center of the computational system, involving the 16th and the 17th crystallographic plane. Simulations were performed at three different temperatures, 20, 40, and 60 K, above the experimental melting point of the noble gas considered. Under such circumstances, an interface-induced melting takes place at the grain boundary. Melting is marked by the nucleation of structural disorder at the interfacial region and its rapid propagation to the adjacent planes. The rate at which the liquid−solid interface propagates was evaluated by means of the planar static order parameter $S_p(\mathbf{k})$, defined as

$$S_p(\mathbf{k}) = \frac{1}{N_p}\{[\sum_{i=1}^{N_p}\cos(\mathbf{k}\mathbf{r}_i)]^2 + [\sum_{i=1}^{N_p}\sin(\mathbf{k}\mathbf{r}_i)]^2\}^{1/2} \tag{2}$$

where the wave vector $\mathbf{k}$ is a reciprocal lattice plane vector, $\mathbf{r}_i$ is the vector defining the position of the ith atom in the plane, and N_p is the total number of atoms in the plane. $S_p(\mathbf{k})$ describes and quantifies the breakdown of long-range crystalline order in atomic planes.[23] For an ideal crystal at zero temperature, $S_p(\mathbf{k})$ equals unity for any wave vector $\mathbf{k}$. By contrast, in the liquid state or in a completely amorphous solid $S_p(\mathbf{k})$ values are close to zero. $S_p(\mathbf{k})$ thus provides a direct quantitative measure of the overall disorder of the system under investigation. The degree of disorder was evaluated along the crystallographic directions [111].

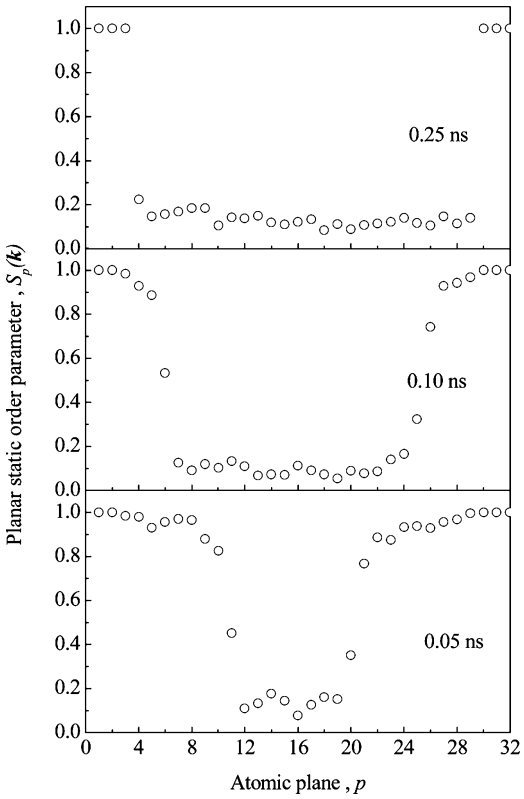

Figure 1. Planar static order parameter $S_p(\mathbf{k})$ is reported for each crystallographic plane after 1000, 5000, and 9000 time steps. Data refer to fcc Ar at a temperature of 124 K. The gradual disappearance of the long-range order as the liquid−solid interface propagates in the direction perpendicular to the (γ29) high-angle grain boundary. It appears that the rate of propagation of the liquid−solid interface is about 60 m s^{-1}.

The propagation rate ω depends on the system temperature. The equilibrium melting temperature T_m was identified with the temperature at which the propagation rate ω vanishes.[28,29] The melting point obtained according to such procedure, even though considerably closer to the thermodynamic melting point than the temperature T_m^K, corresponding to the first limit to superheating, does not yet reproduce the experimental melting point. The melting point estimate depends, indeed, on a number of factors such as grain boundary stability and system size. For example, the (γ29) high-angle twist boundary used here is characterized by a relatively marked kinetic instability and leads to an underestimation of the melting temperature. As explained in previous works,[28,29] a better estimate could be obtained by averaging the melting temperatures obtained from systems containing different low-angle and high-angle grain boundaries.

The high-angle twist boundary allows for the heterogeneous nucleation of molten phase to occur. Irrespective of the temperature at which calculations are carried out, a disordered interface is rapidly formed. As evident from Figure 1, where the values of the static order parameter $S_p(\mathbf{k})$ for each crystallographic plane p are quoted at different times, the disorder propagates in the direction perpendicular to the (001) interface. The rate of propagation ω depends on the temperature at which propagation occurs. It can be seen from Figure 2 that the propagation rate ω increases with the temperature, T. A quadratic

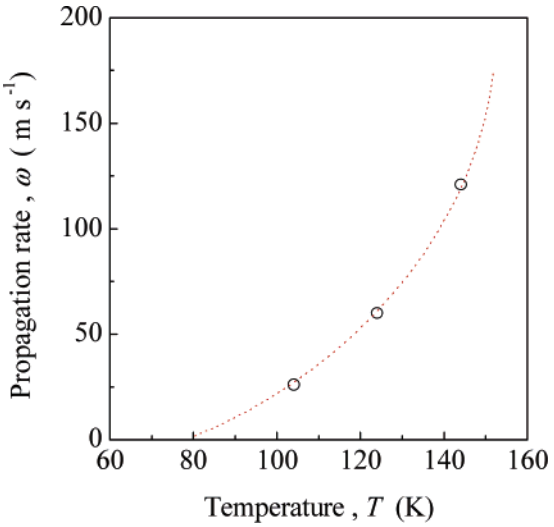

Figure 2. Rate, ω, of propagation of the liquid−solid interface as a function of the temperature, T. The rate increases as the temperature increases. The best-fitted quadratic curve is also shown. An equilibrium melting temperature, T_m, of about 80 K is obtained. Data refer to fcc Ar.

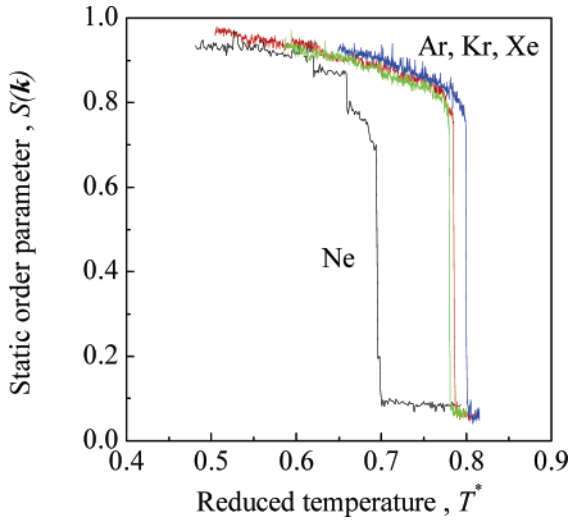

Figure 3. Static long-range order parameter $S(\mathbf{k})$ as a function of the temperature, T^*, for the chemical species indicated. In all of the cases, a sudden downward jump is observed after a gradual decrease. The sudden drop identifies the temperature, T_m^K*, at which homogeneous melting occurs.

TABLE 2: Experimental Melting Points T_m^{exp}, the Equilibrium Melting Points T_m, Estimated by Numerical Simulation, the Homogeneous Melting Points T_m^K, and Their Ratio T_m^K/T_m for the Chemical Species Investigated[a]

element	T_m^{exp}, K	T_m, K	T_m^K, K	T_m^K/T_m
Ne	24.5	19.4 (0.54)	22.6 (0.64)	1.16
Ar	83.8	80.3 (0.67)	93.5 (0.78)	1.16
Kr	115.9	108.7 (0.63)	134.5 (0.78)	1.23
Xe	161.2	149.5 (0.67)	182.2 (0.81)	1.21

[a] Melting points in reduced units are reported in parentheses. The average superheating is equal to 1.19.

fit was carried out to approximately determine the temperature at which the propagation rate is equal to zero, which corresponds to the equilibrium melting temperature, T_m.

The equilibrium melting temperatures obtained from calculations are reported in Table 2 together with the experimental values. It can be seen that the calculated temperatures are, on the average, about 3−10 K lower than the experimental ones. The largest difference pertains to Ne, about 10 K, and the smallest one pertains to Ar, about 5 K. As briefly mentioned before, a certain variability in the estimated melting point can be expected depending on the system size as well as on the defective site, for example, free surfaces, grain boundaries, and point defects, at which the melting process heterogeneously nucleates.[28,29] The present paper only analyzes the behavior of the so-called (γ29) high-angle twist boundary, a highly mobile boundary that can give rise to interface migration and reconstruction. It is therefore reasonable to expect that a different grain boundary could yield a different estimate of the melting point. The values obtained in the present work should thus be considered at best good estimates of the equilibrium melting points for the conditions under which simulations have been actually carried out.

Homogeneous melting. The first limit to superheating, corresponding to the homogeneous melting point T_m^K, was evaluated by applying the so-called periodic boundary conditions along the three Cartesian directions to simulate a defect-free crystalline bulk.[23] Under such circumstances, considerable degrees of superheating can be attained, and the dynamics in the vicinity of the first limit to superheating can be properly investigated.

The initial structure consisting of 6912 atoms was equilibrated for 2×10^4 time steps at an external pressure $P \approx 0$ and a temperature $T = 0.3T_m$, where T_m is the numerically estimated equilibrium melting point for the potential used. After the equilibration stage, the temperature was slowly raised with a step-by-step procedure. In particular, temperature jumps $\Delta T = 0.05$ K were imposed in a single step, followed by equilibration stages of 2500 time steps. The mechanical melting of the cF4 structure was finally obtained at temperatures T_m^K depending on the characteristic properties of each chemical species. Such temperatures are reported for each chemical species in Table 2.

Long-range crystalline order was monitored by means of the static order parameter $S(\mathbf{k})$,[23] which represents the three-dimensional analogue of the planar static order parameter defined in eq 2. Of course, $S(\mathbf{k})$ equals unity for an ideal crystal at 0 K and assumes small positive values for liquid and amorphous phases. Structural order was also monitored by means of the radial distribution function (RDF).[23]

The gradual temperature increase determines a corresponding gradual change of the system properties as a consequence of the increased thermal disordering. Due to the absence of free surfaces and interfaces, the occurrence of melting at the equilibrium melting point, T_m, is systematically suppressed. Melting occurs, instead, under superheating conditions, that is, at a characteristic temperature, T_m^K, higher than the equilibrium melting point. At T_m^K, the crystalline lattice reaches the maximum degree of superheating allowed by the rate of temperature increase and loses its characteristic long-range order, forming a molten phase.

The increase of thermal motion of atomic species around their equilibrium lattice positions induces a gradual, although limited, loss of the long-range order characteristic of a crystalline lattice. This, in turn, determines a gradual decrease of the static order parameter $S(\mathbf{k})$. The $S(\mathbf{k})$ values for the four chemical species considered are reported in Figure 3 as a function of the reduced temperature, T^*. With the exception of Ne, the curves pertaining to the different chemical species investigated show a definite superposition, thus indicating that the species undergo a similar behavior. The deviation from the common trend of the curve

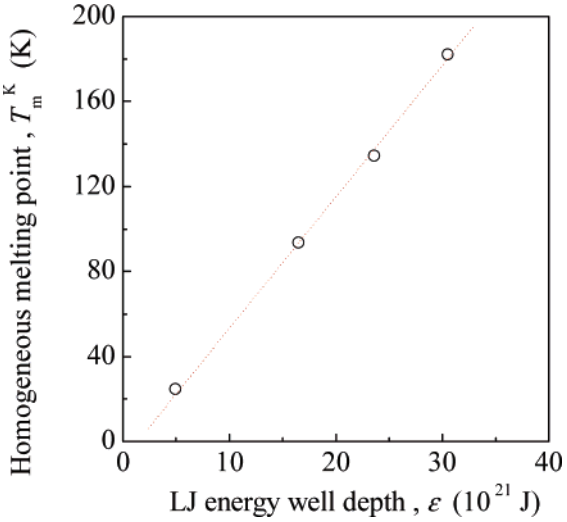

Figure 4. Homogeneous melting point, T_m^K, also referred to as the limit of superheating, as a function of the energy well depth ϵ of the LJ potential. A definite linear proportionality is observed. The best-fitted line is also shown.

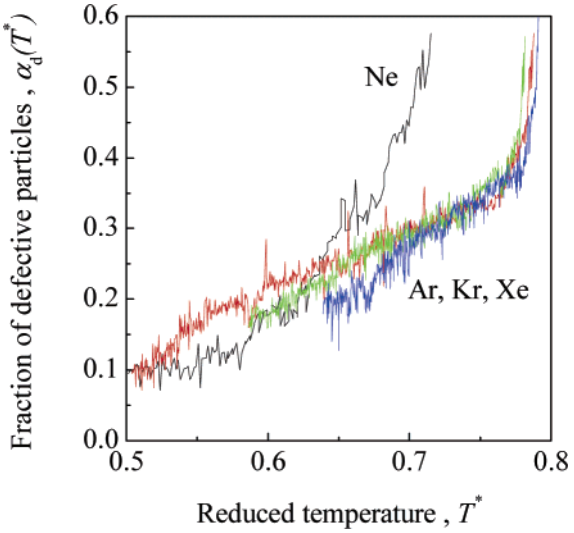

Figure 5. Fraction of defective atoms, $\alpha_d(T^*)$, as a function of the reduced temperature, T^*, for the four chemical species considered. Irrespective of the chemical species, at homogeneous melting ad amounts approximately to 0.4. The $\alpha_d(T^*)$ curves superpose almost perfectly with the exception of Ne.

of Ne can be explained by the fact that quantum corrections should be carried out to the LJ potential to satisfactorily reproduce the experimental physical behavior of Ne. It can be seen that $S(\mathbf{k})$ undergoes an almost linear decrease up to a temperature on the order of the expected T_m^*. Successively, the decrease assumes a more and more nonlinear character until a sudden drop to values close to zero takes place. The drop identifies the temperature at which the crystalline lattice can no longer be equilibrated and then the limit of superheating, T_m^K*. At such a temperature, the crystal melts homogeneously, as confirmed by the shape of calculated RDF (not shown).

The temperature T_m^K* at which melting takes place is characteristic of each chemical species. In particular, it depends on the LJ energy well depth ϵ. As shown in Figure 4, an approximately linear trend is obtained when the temperatures T_m^K are reported as a function of ϵ. This indicates the existence of a scaling behavior between the limit of superheating, T_m^K, and the properties of the different chemical species considered.

The conventional elastic constants were calculated to monitor the gradual change of the elastic properties of crystalline lattices investigated. To save computational time, calculations were restricted to the elastic constants C_{11} and C_{12}, which allow for an indirect estimate of the shear modulus $C' = (C_{11} - C_{12})/2$. The usual method for quantifying the so-called Born and fluctuation contributions at constant pressure was applied.[30,31] For the sake of brevity and due to the lack of novelty in the elastic behavior observed, the latter will not be discussed in detail. The values of shear modulus C' at approximately 2 K amount to 0.32 GPa for Ne, 0.6 GPa for Ar, 0.79 GPa for Kr, and 0.95 GPa for Xe, whereas the ones obtained at the homogeneous melting are equal to 0.13 GPa for Ne, 0.33 GPa for Ar, 0.36 GPa for Kr, and 0.446 GPa for Xe. These values will be used in the discussion of the results.

Topological Defects and Homogeneous Melting. The formation of defective structures in the originally defect-free bulk was pointed out by monitoring the appearance of atoms with a number of nearest neighbors different from 12, which is the normal coordination number in fcc lattices. The number of nearest neighbors was evaluated for each atom according to a distance criterion. Two atoms were thus regarded as nearest neighbors when their distance was lower than the one, r_{min}, corresponding to the first minimum of RDF. Two different atom subsets can be therefore identified within the crystalline system, the larger one including 12-fold coordinated atoms and the smaller one consisting of atoms with a number of nearest neighbors different from 12, hereafter referred to as defective atoms.

The fraction of defective atoms, $\alpha_d(T^*)$, defined as the ratio between the number of defective atoms and the total number of atoms in the system, is quoted in Figure 5 as a function of temperature T^*. The fraction $\alpha_d(T^*)$ undergoes a gradual increase with temperature. The increase is linear for all of the chemical species up to a temperature on the order of (0.7−0.8) T_m^K*, above which nonlinearity becomes evident. The curves in Figure 5, except for Ne, extensively superpose. Irrespective of the chemical species considered, at homogeneous melting $\alpha_d(T^*)$ assumes a value $\alpha_d(T_m^K*)$ of about 0.4.

The appearance of defective atoms is correlated to the occurrence of thermal vibrations. As the amplitude of thermal vibrations increases, neighboring atoms begin to reciprocally hinder their motion. Under such circumstances, the formation of atoms with defective coordination seems to be somehow favored. The nearest-neighbors' shells of the two nearest-neighbor atoms undergo a local rearrangement resulting in the formation of pairs of defective atoms consisting of 11-fold and 13-fold coordinated atoms. Atoms with different defective coordinations, for example 14-fold or 10-fold coordination, are rarely observed and only for very short times. At relatively low temperatures, defective atom pairs appear randomly in the bulk and remain distant from other pairs eventually present. At higher temperatures, however, the mechanism leading to the formation of defective atoms becomes cooperative and the pairs of defective atoms are generated in the neighborhood of preexisting ones. As a consequence, at temperatures on the order of (0.5−0.6)T_m^K*, defective atoms begin to form extended pseudolinear clusters, such as the ones shown in Figure 6a,b.

The same distance criterion mentioned above was also applied to investigate the spatial correlation between defective atoms. These can indeed form agglomerates or groups in which neighboring defective atoms are strongly correlated. To evaluate the total number of clusters $N_{cl}(T^*)$ of defective atoms present in the system and their size, two defective atoms were regarded as belonging to the same cluster when their distance was shorter

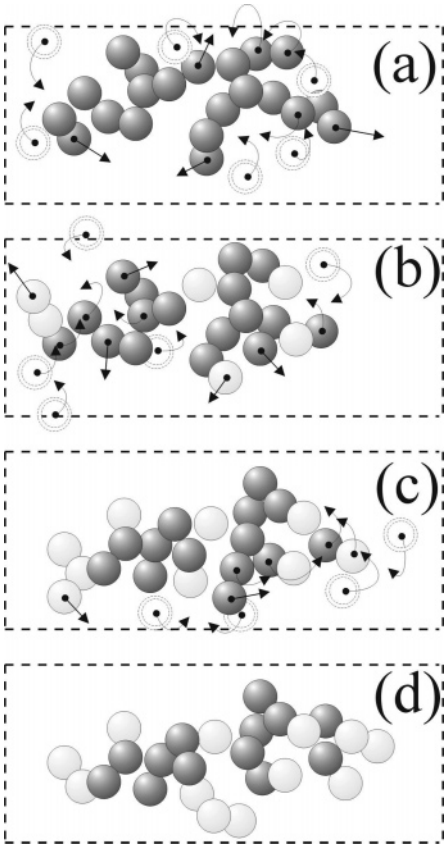

Figure 6. (a) Planar projection of a cluster of Ar defective atoms at $T \approx 80$ K. (b), (c), and (d) Same cluster after 200, 500, and 800 ps, respectively. Dark gray marks the atoms already belonging to the cluster at the beginning of the 800 ps time interval. Light gray marks those atoms not belonging to the cluster at the beginning of the time interval considered. Dashed double circles indicate, irrespective of their coordination number, the atoms that are going to become connected with the cluster. Curved arrows approximately indicate either the displacement of defective atoms within the cluster or the joining of new atoms to the cluster. Linear arrows approximately indicate the direction along which a defective atom leaves the cluster restoring a normal coordination. Dashed lines mark the region of solid considered and can be used as a reference framework to evaluate the configurational and positional change of the cluster. It is possible to see that the cluster dynamics is characterized by a continuous displacement and replacement of atoms.

than r_{min}. Although it has been suggested that these clusters should be regarded as dislocation lines,[22] it is necessary to point out some interesting aspects.

In the first place, not all of the stringlike clusters formed by defectively coordinated atoms have the properties of actual dislocation lines. Let us consider, for example, the case of atomic configurations at the early stages of simulation. A small number of defective atoms exists, randomly dispersed in the bulk. Defective atoms appear in pairs as a consequence of the mechanism of generation, which involves the rearrangement of nearest-neighbors' shells of nearest-neighbor atoms. An isolated pair of defectively coordinated atoms is nothing other than a transient bulk defect. The term transient refers to the evidence that defective atoms have lifetimes depending on various factors among which temperature seems to play the most important role. In principle, any atom in the system can undergo a nearest-neighbors' shell rearrangement and assume a defective coordination. Such defective coordination is maintained until a thermal fluctuation induces a rearrangement of nearest neighbors and permits the recovery of a 12-fold coordination. The atom can become repeatedly involved in similar rearrangement processes and accordingly change its coordination. At low temperature, the lifetimes of defective atoms are relatively long, on the order of 10 ns. As the temperature increases, the lifetimes become shorter and shorter and attain values of about 1 ns at the homogeneous melting point.[32] However, at high temperatures, the number of defective atoms is significantly larger than at low temperatures, and the defective atom pairs interact with each other, forming stringlike, fractal clusters. Such clusters occasionally display properties characteristic of dislocations. In particular, Shockley partial dislocations with a (111) glide plane moving irregularly in the [110] and one of the [211] crystallographic directions have been observed. The formation of stacking faults has been also observed by monitoring the local crystalline order by means of the so-called Honeycutt−Andersen parameters.[32] More specifically, crystalline domains of about 30 atoms on the average with the hexagonal-close-packed (hcp) arrangement have been detected, surrounded by small dislocation loops. In the vicinity of the homogeneous melting point, open dislocation lines crossing the whole system have been also observed, still with a (111) glide plane. In addition, configurations of 12 nearest-neighbor atoms with 11-fold as well as with 13-fold coordination have been observed, corresponding respectively to vacancies and interstitial atoms. It is, however, difficult to report a detailed statistical analysis of the number of dislocations and dislocation loops observed at each temperature. Defective atoms are indeed subjected to a fast dynamics, and defective atom clusters correspondingly undergo fast modifications in both size and position. A preliminary analysis on atomic coordinates at 0.4-, 0.6-, and $0.8T_m^K*$ reveals that the percentage of defective atom clusters displaying dislocation or other defect properties amounts approximately to 14%, 31%, and 47%, respectively. The number of identifiable dislocations increases then with temperature. Further work is, however, necessary to satisfactorily address this important point.

The fundamental characteristics of such rearrangements can be easily understood by analyzing in detail the dynamics of a single defective atom and its neighbors. Let us consider, for the sake of illustration, the case of an 11-fold coordinated atom, hereafter referred to as the *A* atom, at the temperature $0.8T_m^K*$. *A* is surrounded by two 13-fold coordinated atoms, referred to as *B* atoms, eight 12-fold coordinated atoms, referred to as *C* atoms, and one 11-fold coordinated atom, referred to as the *D* atom. *A* keeps its defective coordination for about 710 ps. Successively, it acquires one more neighbor from one of the 13-fold coordinated nearest-neighbors *B*. The *B* atom as well as the *A* atom become then 12-fold coordinated. After about 230 ps, the *A* atom, which was originally 11-fold and then became 12-fold coordinated, participates in a new local rearrangement of the nearest-neighbors' shells and assumes again an 11-fold coordination. This time, however, *A* is surrounded by only one 13-fold coordinated atom and 10 12-fold coordinated ones. *A* returns to the normal 12-fold coordination after 550 ps. After an additional 370 ps, it becomes once more defective, but with 13 nearest neighbors. The dynamic evolution of the nearest-neighbors' shell of the *A* atom, as well as those of all of the other atoms in the system, takes place throughout the simulation.

As briefly mentioned before, in principle all of the atoms belonging to the system can undergo the processes briefly described above for the *A* atom. In practice, however, the rate of nearest-neighbors' shell modification is much higher for those atoms that either are themselves defective or are neighbors of defective atoms. In this case, nearest-neighbors' shells undergo

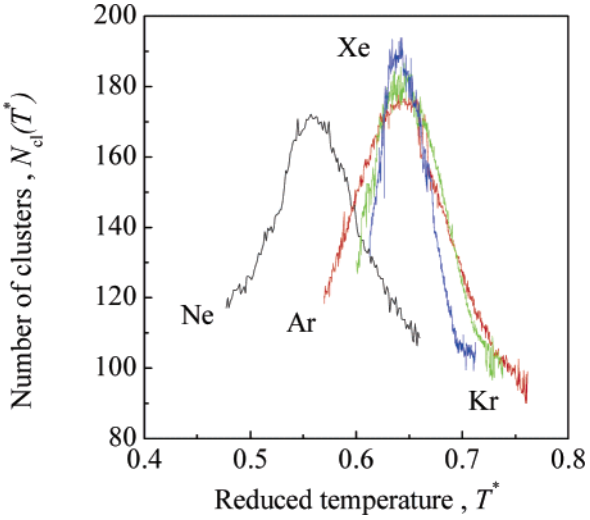

Figure 7. Number of clusters, $N_{cl}(T^*)$, of defective atoms as a function of the reduced temperature, T^*, for the four chemical species considered. Except for Ne, a net superposition of $N_{cl}(T^*)$ curves is observed. The final part of the curves arriving at T_m^K* is not shown for sake of clarity, being characterized by strong fluctuations around an average value.

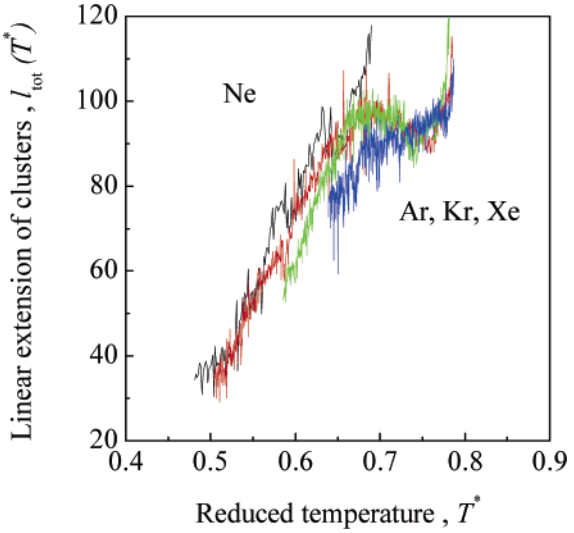

Figure 8. Total linear extension, $l_{tot}(T^*)$, as a function of the reduced temperature, T^*. The curves pertaining to the four chemical species are considered superposed.

a continuous change that determines, in turn, a continuous change in the number and identity of defective atoms.

Accordingly, a continuous change in the position and configuration of the clusters of defective atoms is observed. The situation is clearly illustrated by the two cluster configurations reported in Figure 6a,b. The figures depict the same cluster, that is, the cluster present in a certain region of solid, at two different times at the temperature $0.8T_m^K*$. The two times are separated by only 800 ps. Within such a time interval, the cluster has maintained its average position, whereas the number and the identity of the atoms involved have changed.

The dynamics of defective atoms provides a mechanism for clusters to interact and undergo ramification as well as fragmentation and coalescence processes. The number $N_{cl}(T^*)$ of clusters and the size of each cluster, that is, the number of defective atoms involved in the chainlike structures, depend on temperature. It can be seen from Figure 7, where the number of clusters, $N_{cl}(T^*)$, is reported as a function of temperature T for all of the chemical species considered, that $N_{cl}(T^*)$ initially increases, reaches a maximum value, and finally decreases. The behavior observed is the same for all of the chemical species, and the various curves superpose as in the case of $\alpha_d(T^*)$.

The occurrence of a maximum is related to the gradual increase of the average cluster size with temperature. Initially, the number of clusters, $N_{cl}(T^*)$, undergoes a relatively fast increase due to the increase in the fraction of defective atoms, $\alpha_d(T^*)$. At lower temperatures, it is highly probable that defective atom pairs appear as isolated pairs, that is, in positions apparently independent of those of other defective atoms. However, as the temperature and then the number of defective atoms increase, it becomes more and more probable that new defective atom pairs appear as neighboring atoms of preexisting defective atoms. In this case, the appearance of the defective atom pair does not determine an increase of the cluster number but of the cluster size. This provides a mechanism limiting the growth of the cluster number $N_{cl}(T^*)$ because the increase in the cluster size favors the interaction and connection of clusters. Thus, at a relatively high temperature, cluster coalescence processes become the most probable ones and induce a gradual decrease of the total number of clusters, $N_{cl}(T^*)$. These then become bigger, but their number decreases.

Cluster size and spatial extension are interrelated and temperature-dependent. At any temperature T^*, the size $n_j(T^*)$ of the jth cluster determines its linear extension $l_j(T^*)$. The latter quantity can be defined as a function of the number of "bonds" in the cluster. The term "bond" identifies the distance between two nearest-neighbor atoms belonging to the same cluster. If the number of defective atoms in the jth cluster is $n_j(T^*)$, the number of distances between nearest neighbors, or bonds, is $n_b(T^*) = n_j(T^*) - 1$. The linear extension $l_j(T^*)$ of the jth cluster can then be defined as the sum of all of the bond lengths or distances between nearest neighbors, d_b, in the cluster, that is,

$$l_j(T^*) = \sum_{b=1}^{n_b(T^*)} d_b \tag{3}$$

The total linear extension of defective atom clusters, $l_{tot}(T^*)$, can be therefore defined as

$$l_{tot}(T^*) = \sum_{j=1}^{N_{cl}(T^*)} l_j(T^*) \tag{4}$$

This quantity permits the evaluation of the defective atom cluster density, $\rho(T^*)$, at temperature T^*, defined as the ratio between $l_{tot}(T^*)$ and the volume, $v(T^*)$. The $l_{tot}(T^*)$ values are reported in Figure 8 as a function of the reduced temperature, T^*. As in the cases of $\alpha_d(T^*)$ and $N_{cl}(T^*)$, the curves pertaining to the four different chemical species superpose almost perfectly. It can be seen that, irrespective of the chemical species considered, homogeneous melting occurs when the total linear extension of defective atom clusters reaches on the average the value of about 113 ± 5 (in reduced units) or $71a \pm 3a$ (where a is the cell parameter). In the case of Ar, this corresponds to about 40 nm.

Of course, a superposition is also observed in Figure 8, where the total linear extension $l_{tot}(T^*)$ is reported as a function of the reduced temperature T^*. These evidences once more indicate that the four chemical species investigated display analogue behavior when subjected to temperature increase. When homogeneous melting takes place, at the characteristic temperatures T_m^K*, the systems are characterized by approximately the same fraction of defective atoms, $\alpha_d(T^*)$, the same number of clusters, $N_{cl}(T^*)$, and the same linear extension, $l_{tot}(T^*)$. This finding

clearly provides qualitative support for the conclusions of Burakovsky et al. in their work on the statistical mechanics of dislocation loops.[21] According to their model, the dislocation density, $\rho_{dis}(T^*_m)$, for the noble gases at the melting point is approximately the same, which is in qualitative agreement with the results of the simulations. Their numerical results, however, indicate that the four noble gases Ne, Ar, Kr, and Xe melt when $\rho_{dis}(T^*_m)$ is equal to 0.63 ± 0.2 (in reduced units) or $1.6a^{-2} \pm 0.4a^{-2}$. This value, which can be said to characterize the solid-to-liquid transition of noble gases, is relatively far from the one obtained in the present work from computer simulations. Calculations yield a pseudolinear cluster density $\rho(T^K_m*)$ of about $0.016 \pm (8 \times 10^{-4})$ (in reduced units), obtained by dividing the total linear extension of cluster, $l_{tot}(T^K_m*) \approx 113 \pm 5$, by the system volume, about $(19)^3$, at the onset of homogeneous melting. The $\rho(T^K_m*)$ value of about 0.016 is remarkably lower than the $\rho_{dis}(T^*_m)$ value of about 0.63 predicted by Burakovsky et al.[21] The reasons for such discrepant $\rho(T^K_m*)$ and $\rho_{dis}(T^*_m)$ values can be found in the differences existing between the assumptions underlying the original approach of Burakovsky et al.[21] and the conditions under which the calculations are carried out. These aspects deserve a detailed comment.

The first point worth noting is that the model of Burakovsky et al. describes dislocations as noninteracting, closed loops on a crystalline lattice.[21] This is an important difference with regard to MD simulations, where all of the pseudolinear clusters observed are considered, although only a fraction of them display properties characteristic of dislocations. Moreover, the evaluation of the dislocation density at melting is based on the assumption that the crystalline lattice instability related to the vanishing of the work necessary for creating dislocation loops manifests itself at the experimental melting point T_m.[21] Such an assumption therefore implies that the model is referred to as a heterogeneous melting scenario in which the molten phase, or the dislocation lines, nucleate preferentially at defective lattice sites. This is, however, in contradiction with the fact that all of the lattice sites are considered equivalent.[21] No mechanism for the heterogeneous generation of closed loops is thus introduced in the model. Under such circumstances, that is, equivalent lattice sites, it seems to be quite reasonable to refer the model to a homogeneous melting scenario rather than to a heterogeneous one. Thus, the temperature at which the lattice instability sets in should coincide with the limit of superheating, T^K_m, and not with the thermodynamic melting point, T_m. Finally, Burakovsky et al. calculated the dislocation line density by using room-temperature values of the shear modulus C'.[21] Therefore, their calculations did not take into account the elastic softening of the crystalline structure occurring when the crystal undergoes a temperature increase, which can induce a decrease of the shear modulus C' as pronounced as 40−50%.

The previous points can be roughly taken into account in the model of Burakovsky et al. without modifying the fundamental aspects. To carry out a proper comparison between numerical simulation results and theoretical predictions, it is only necessary to repeat the calculation of the dislocation density, $\rho_{dis}(T^K_m*)$, with the proper values of melting temperature and of shear modulus, that is, the limit of superheating, T^K_m*, and the softened C' value at T^K_m*. Under such conditions, an average dislocation density, $\rho_{dis}(T^K_m)$, of about 0.05 is obtained. This value is considerably closer to the one (0.016) obtained from calculations than to the one (0.63) originally indicated by Burakovsky et al. Taking into account the various differences between the methods employed to evaluate the calculated $\rho(T^K_m*)$ and theoretical $\rho_{dis}(T^K_m*)$ values, such evidence seems to suggest that the model developed by Burakovsky et al. works relatively well when applied to the case of homogeneous melting at the limit of superheating. On such a basis, it seems possible that, in agreement with the initial hypothesis of Burakovsky et al.,[21] the instability leading to the collapse of the crystalline structure at the limit of superheating could be essentially a dislocation-mediated process. As a consequence, homogeneous melting at the limit of superheating should be regarded as a dislocation-mediated phase transition.

Conclusions

The four noble gases investigated display a similar behavior. The thermodynamic melting is systematically bypassed and the solid-to-liquid transition takes place under metastable superheating conditions. The temperature at which the crystalline lattices undergo the homogeneous phase transition depends on the energy well depth of the LJ potential. In all of the cases, the thermal disorder determines the formation of pairs of atoms with defective coordination. The increase of the number of defective atoms with temperature gradually favors the formation of stringlike clusters of various sizes. At melting, the total linear extension of clusters, scaled with respect to the elementary cell parameter for the sake of comparison, is the same for all of the species. Correspondingly, the density of dislocations, expressed as a function of the elementary cell parameter, is also approximately the same for all of the noble gases.

Such a finding seems to validate the theoretical model developed by Burakovsky et al.,[21] provided that it is applied to the case of a homogeneous melting scenario. Under such conditions, a relatively good agreement between model predictions and computer simulation results is found despite the deep differences between the two approaches. It is therefore reasonable to conclude that the theoretical model developed by Burakovsky et al. should not be applied to thermodynamic melting, as originally claimed, but to the homogeneous nucleation of molten phase in the crystalline bulk. As a consequence, the homogeneous melting at the limit of superheating can be regarded as a dislocation-mediated phase transition.

Further work is necessary to explore the various implications of such a finding.

Acknowledgment. The University of Cagliari is acknowledged for financial support. Professor G. Cocco, Dipartimento di Chimica, Università degli Studi di Sassari, is gratefully acknowledged for useful discussions.

References and Notes

(1) Chandler, D. *Introduction to Modern Statistical Mechanics*; Oxford University Press: Oxford, U.K., 1987.
(2) Dash, J. G. *Contemp. Phys.* **2002**, *43*, 427.
(3) Atkins, P. W. *Physical Chemistry*; Oxford University Press: Oxford, U.K., 1990.
(4) Lindemann, F. A. *Z. Phys.* **1910**, *11*, 609.
(5) Gilvarry, J. J. *Phys. Rev.* **1956**, *102*, 308.
(6) Born, M. *J. Chem. Phys.* **1939**, *7*, 591.
(7) Born, M.; Huang, K. *Dynamical Theory of Crystal Lattices*; Clarendon Press: Oxford, U.K., 1954.
(8) Tallon, J. L. *Nature* **1989**, *342*, 658.
(9) Cormia, R. L.; Mackenzie, J. D.; Turnbull, D. *J. Appl. Phys.* **1963**, *34*, 2239.
(10) Cahn, R. W. *Nature* **1986**, *323*, 668.
(11) Maddox, J. *Nature* **1987**, *330*, 599.
(12) Daeges, J.; Gleiter, H.; Perepezko, J. H. *Phys. Lett. A* **1986**, *119*, 79.
(13) Zhang, D. L.; Cantor, B. *Acta Metall. Mater.* **1991**, *39*, 1595.

(14) Wolf, D.; Okamoto, P. R.; Yip, S.; Lutsko, J. F.; Kluge, M. *J. Mater. Res.* **1990**, *5*, 286.
(15) Lu, K.; Li, Y. *Phys. Rev. Lett.* **1998**, *80*, 4474.
(16) Jin, Z. H.; Gumbsch, P.; Lu, K.; Ma, E. *Phys. Rev. Lett.* **2001**, *87*, 055703.
(17) Kosterlitz, J. M.; Thouless, D. J. *J. Phys. C: Solid State Phys.* **1973**, *6*, 1181.
(18) Nelson, D. R.; Halperin, B. I. *Phys. Rev. B* **1979**, *19*, 2457.
(19) Young, A. P. *Phys. Rev. B* **1979**, *19*, 1855.
(20) Kleinert, H. *Gauge Theory in Condensed Matter*; World Scientific: Singapore, 1989.
(21) Burakovsky, L.; Preston, D. L.; Silbar, R. R. *Phys. Rev. B* **2000**, *61*, 15011.
(22) Gomez, L.; Dobry, A.; Geuting, C.; Diep, H. T.; Burakovsky, L. *Phys. Rev. Lett.* **2003**, *90*, 095701.
(23) Allen, M. P.; Tildesley, D. *Computer Simulation of Liquids*; Clarendon Press: Oxford, U.K., 1987.
(24) Broughton, J. Q.; Gilmer, G. H. *J. Chem. Phys.* **1983**, *79*, 5095.
(25) Andersen, H. C. *J. Chem. Phys.* **1980**, *72*, 2384.
(26) Nosè, S. *J. Chem. Phys.* **1984**, *81*, 511.
(27) Parrinello, M.; Rahman, A. *J. Appl. Phys.* **1981**, *52*, 7182.
(28) Wolf, D.; Okamoto, P. R.; Yip, S.; Lutsko, J. F.; Kluge, M. *J. Mater. Res.* **1990**, *5*, 286.
(29) Phillpot, S. R.; Lutsko, J. F.; Wolf, D.; Yip, S. *Phys. Rev. B* **1989**, *40*, 2831.
(30) Ray, J.; Rahman, A. *J. Chem. Phys.* **1984**, *80*, 4423.
(31) Ray, J.; Rahman, A. *Phys. Rev. B* **1985**, *32*, 733.
(32) Honeycutt, J. D.; Andersen, H. C. *J. Phys. Chem.* **1987**, *91*, 4950.